

Experimental and Numerical Analysis of the Bulk Flow Parameters Within an Arteriovenous Fistula

LEONARD D. BROWNE, MICHAEL T. WALSH, and PHILIP GRIFFIN

Department of Mechanical, Aeronautical and Biomedical Engineering, Materials and Surface Science Institute, Centre for Applied Biomedical Engineering Research (CABER), University of Limerick, Limerick, Ireland

(Received 20 June 2015; accepted 16 September 2015; published online 23 September 2015)

Associate Editor Ajit P. Yoganathan oversaw the review of this article.

Abstract—The creation of an arteriovenous fistula for hemodialysis has been reported to generate unstable to turbulent flow behaviour. On the other hand, the vast majority of computational fluid dynamic studies of an arteriovenous fistula use low spatial and temporal resolutions resolution in conjunction with laminar assumptions to investigate bulk flow and near wall parameters. The objective of the present study is to investigate if adequately resolved CFD can capture instabilities within an arteriovenous fistula. An experimental model of a representative fistula was created and the pressure distribution within the model was analysed for steady inlet conditions. Temporal CFD simulations with steady inflow conditions were computed for comparison. Following this verification a pulsatile simulation was employed to assess the role of pulsatility on bulk flow parameters. High frequency fluctuations beyond 100 Hz were found to occupy the venous segment of the arteriovenous fistula under pulsatile conditions and the flow within the venous segment exhibited unstable behaviour under both steady and pulsatile inlet conditions. The presence of high frequency fluctuations may be overlooked unless adequate spatial and temporal resolutions are employed. These fluctuations may impact endothelial cell function and contribute to the cascade of events leading to aggressive intimal hyperplasia and the loss of functionality of the vascular access.

Keywords—Instabilities, Computational fluid dynamics, Pressure drop, Arteriovenous fistula, Vascular access dysfunction.

INTRODUCTION

The creation of an arteriovenous fistula is formed by the direct anastomosis of an artery to a vein. This newly formed fistula will undergo substantial remodelling in response to the increased blood flow as a result of the large pressure gradient between the artery and vein. There is a general consensus that the hemodynamic changes that occur after the construction of the fistula play an important role in regulating the structural vascular response thereafter. Numerical models have been utilised to study the interaction between hemodynamic profiles and remodelling within arteriovenous fistulae. Clarifying the relationship between vascular remodelling and hemodynamic forces requires accurate measurements of physiological parameters and a detailed 3D analysis of the hemodynamics of the flow. The latter aspect has been hindered, in part, due to the complex flow patterns which are known to arise within the anastomosis with unstable and transitional to turbulent flow reported *in vivo* and *in vitro*.^{9,17} This is an aspect that appears divided or overlooked within the computational modelling community and is likely due to the inherent difficulty associated with resolving such flows. However, certain studies appear to be in direct contradiction to the *in vivo* setting by simulating AVF hemodynamics with the use of low resolution grids and numerical dampening schemes which converge the solution to a stable and laminar state. Their justification arises from the fact that the arterial Reynolds number is below the critical Reynolds number for a straight pipe.^{5,8,15,16} However, deviations in vessel curvature and tortuosity, flow splits and the pulsatile nature of flow can significantly lower this critical Reynolds number.^{3,11} Hence, there is a need for numerical models to replicate clinically detected features such as the instabilities which arise within the anastomosis of

Address correspondence to Philip Griffin, Department of Mechanical, Aeronautical and Biomedical Engineering, Materials and Surface Science Institute, Centre for Applied Biomedical Engineering Research (CABER), University of Limerick, Limerick, Ireland. Electronic mail: philip.griffin@ul.ie

an AVF. These models need to be supported by reliable evidence demonstrating that they can accurately estimate the significant energy losses and subsequent dynamics of the flow. Until an accurate characterisation of the hemodynamics of an arteriovenous fistula is undertaken, it is unlikely that successful therapeutic strategies or interventions to improve maturation and patency will be identified. The aim of this study is to demonstrate that the numerical method employed in this analysis is capable of accurately estimating the bulk flow parameters within an arteriovenous fistula. The pressure drop is one such parameter and is directly linked to the non-linear behaviour and overall resistance of the anastomosis. It is a key feature that is strongly linked to the instabilities that arise at the junction and therefore is an important indicator of the global hemodynamics within a fistula.^{3,4} An experimental model of a representative fistula was created and the pressure drop across the anastomosis was measured. Adequate spatial and temporal resolved CFD simulations are simulated and compared to the experimental results to verify that energy losses across and arteriovenous fistula can be replicated and highlight the ability of the model to capture instabilities within the flow. Decomposition techniques are presented and are used to characterise the presence of these instabilities and provides a method to classify the nature of the bulk flow and near wall parameters within an arteriovenous fistula.

MATERIALS AND METHODS

Fistula Model

The verification is conducted on a representative fistula model. The model geometry is taken from a parametric study by Putjens whom characterised the geometry of radiocephalic and brachiocephalic fistulae 6 weeks post operatively.¹⁴ The three main vessels of

the fistula, the proximal artery, distal artery and the vein were segmented and are defined by the parametric equations in Table 1. The fistula model was created within Creo Parametric (PTC) and the vascular surface described previously was subtracted from a block and additional inlet and outlet ports were added. Once the model was obtained it was converted to STL format. A rapid prototype model was printed in an Object500 Conex 3D printer (Stratasys) using a clear transparent ABS resin (Veroclear, Stratasys). The model was placed in an ultrasonic water bath after printing in order to dissolve any residual material.

In-Vitro Flow conditions

The flow system was designed to provide a steady fully developed flow at the anastomosis inlet. The distal outlet was occluded for simplicity and all flow entering the model exited through the venous outlet. This assumption is not in contrast to physiological flow conditions as the majority of the flow exits via the fistula vein since its resistance is much lower than the peripheral resistance of the distal artery, this path of least resistance can also result in reversed distal artery flow i.e., steal syndrome. Therefore, the assumption is clinically relevant and reduces the complexity of the experimental validation.

A steady flow pump was used to generate a range of flow rates within the system. The dimensionless Reynolds number was computed based on the mean velocity (U) entering the arterial inlet, the diameter (D) of the inlet, the density (ρ), and dynamic viscosity (μ) of the fluid.

$$Re = \frac{\rho U D}{\mu} \quad (1)$$

The fluid in the system was a water/glycerol mixture (99.97%, Fisher Scientific, Ireland) with a ratio of 65:35 by volume, which was created to match the dynamic viscosity of blood. The fluid had a density of 1105 kg/

TABLE 1. Centreline and cross sectional description of the arterial and venous segments of a representative arteriovenous fistula.

Distal artery	Proximal artery	Vein
$\begin{cases} x = 15D_a s \\ y = 0 \\ z = D_a s^2 \\ D = D_a \end{cases}$	$\begin{cases} x = 15D_a s \\ y = 0 \\ z = 0 \\ D = D_a \end{cases}$	$\begin{aligned} x &= 15D_a s \\ y &= 15D_a \left(1 - D_a^{-s^{a-b}}\right) \\ z &= D_a s^2 \\ D &= \begin{cases} D_a + (D_v - D_a) \left(\frac{s}{s^*}\right)^{\left(1 - \frac{s}{s^*}\right)} & 0 < s < s^* \\ D_v & s^* < s < 1 \end{cases} \end{aligned}$

The parameter s ranges from 0 to 1, a number of points n were chosen to describe the centreline such that $\Delta s = 1/n$ and represents the resolution of centreline. D_a and D_v represent the diameters of the artery and vein respectively. Parameters $D_a = 5$ mm, $D_v = 8$ mm, $a = 1$, $b = 1.5$ and $s^* = 0.6$ were used to generate a brachiocephalic fistula.

m^3 and a dynamic viscosity μ of 3.7 mPas at 20.8 °C based on the parameterisation by Cheng.⁷ The solution was agitated and the system was allowed to run prior to collecting data, the experimental setup is shown in Fig. 1 with a detailed view of the 3D printed model.

In-Vitro Measurements

An inline flow sensor (5PXN) was connected upstream of the model inlet, the sensor was coupled to a flow meter module (TS410, Transonic Systems, NY) with its low pass filter setting at 0.1 Hz. The meter which was calibrated for the glycerol/water mixture and had a sufficiently long inflow tube to ensure that flow was fully developed prior to entering the flow meter and

model. Pressure measurements were obtained using two pressure transducers (CTE/CTU9000, SensorTechnics) which were connected to various pressure ports within the fistula model. The pressure drop across the anastomosis is defined as the difference between the pressure in the proximal artery and the vein at ± 0.87 abscissa. The pressure difference between each port and the pressure at 0.87 is also measured to evaluate the distribution within the anastomosis. The temperature of the fluid was measured throughout the validation and was synchronously recorded with each measurement of pressure and flow. All data was obtained using a multi-function data acquisition system (NI USB 6211) and processed using LabVIEW (National Instruments). In order to minimize the uncertainties associated with

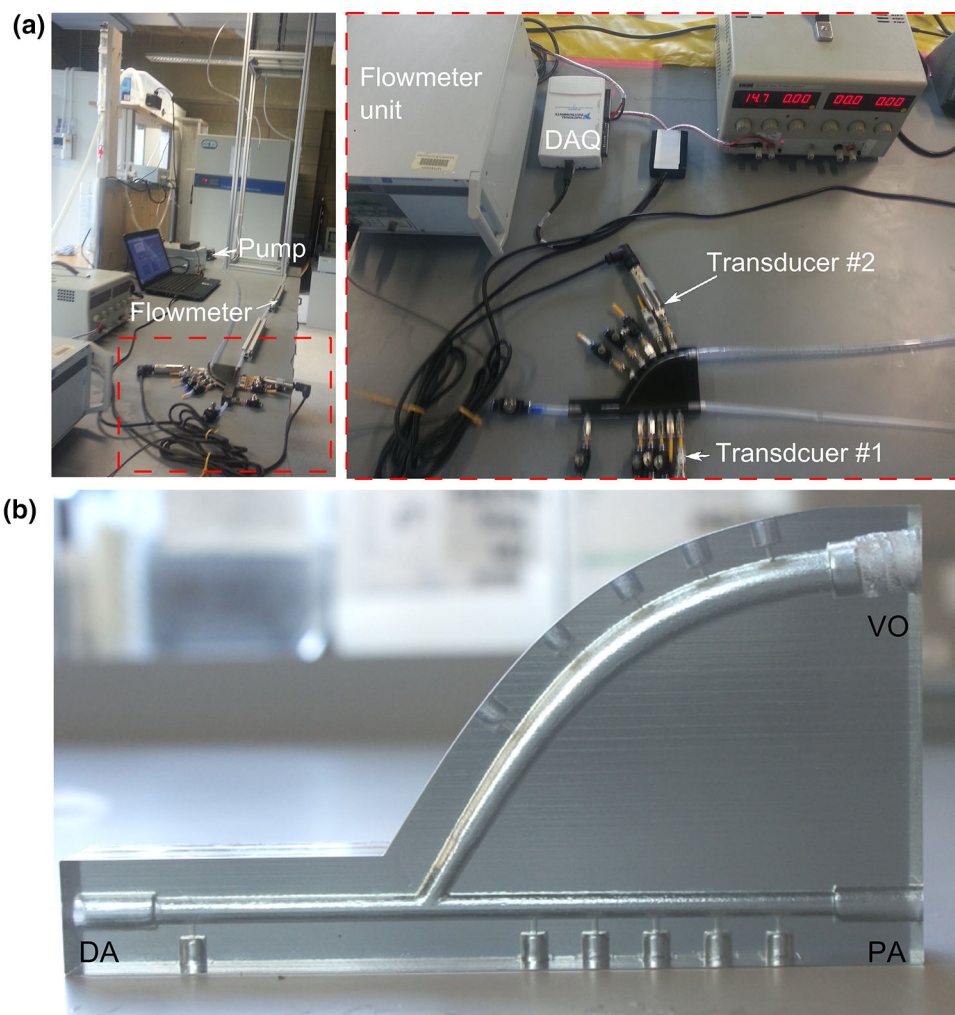


FIGURE 1. The experimental setup is presented in (a). The water/glycerol solution is pumped through the model and returns to the lower reservoir. Two pressure transducers are used to determine the pressure drop across the anastomosis, flow rate is measured upstream of the proximal artery of the model, these signals are acquired by a data acquisition system (DAQ) at the same sampling frequency. The temperature of the fluid is also measured at the same sampling frequency in the system. The 3D printed model of the arteriovenous fistula is shown in more detail in (b), pressure ports are incorporated along the proximal artery and vein, inlet and outlet extensions were also incorporated. PA, DA and VO refer to the proximal artery, distal artery and venous outflow respectively.

experimental error, more than 60 measurements of pressure drop and flow were recorded for each increment in flow.

Numerical Solutions

The fistula geometry was discretised with a structured hexahedral mesh with the package ICFM CFD (Ansys). Three meshes were generated and an H-refinement study was conducted.⁶ The finest mesh had a characteristic edge length of 0.15 mm at the core of the mesh resulting in over 1.7×10^6 cells in the model. The average equiangle skewness and determinant outlined in Table 2 are optimal for CFD applications, further details are provided in supplementary material 1. The unsteady 3D incompressible Navier–Stokes (INS) equations were solved using Star CCM+ (CD Adapco). A segregated approach was adopted to solve these equations for each component of velocity and pressure in an uncoupled manner. A second order scheme is applied for the treatment of the convective term in the momentum equation and a second order backward differentiation scheme is adopted to treat the unsteady term. The flow field for pressure and velocity were initialised with a constant value and simulations were advanced with a time step of 0.5 ms. Both pressure and velocity fields were averaged over all time steps; the first second of data was removed to eliminate transients from solution start up and the simulation reached a physical time of 3 s. A parabolic velocity profile is specified at the arterial inlet with a traction free boundary condition specified at the venous outlet for steady boundary conditions. For pulsatile conditions a brachial artery waveform comprising of 16 harmonic components and one mean component is imposed at the arterial inlet. Rigid boundaries and the no-slip condition are enforced at walls. Blood is modelled as an incompressible Newtonian fluid with material properties matching the *in vitro* validation (Fig. 2).

Data Reduction

Pressure drops are calculated by computing the surface average of each transversal section corresponding to the points where pressure is measured

TABLE 2. Mesh quality metrics of equiangle skewness (Q_{eas}) and determinant (Q_{det}) for the three structured meshes.

Elements	Q_{eas}	Q_{det}
119,000	0.74 (0.24, 0.98)	0.88 (0.55, 1.0)
457,380	0.75 (0.23, 0.98)	0.92 (0.63, 1.0)
1,710,540	0.76 (0.24, 0.98)	0.95 (0.70, 1.0)

Values are presented as mean and (range).

experimentally. The flow regime within an anastomosis is cited as exhibiting transitional or non-laminar behaviour.^{3,12} Under these conditions the flow field exhibits fluctuations and unstable behaviour with the presence of eddies and vortices of many scales. It is necessary to isolate and identify the mechanisms by which flow instabilities affect the mean flow. In order to analyse these interactions and provide a coherent description of the flow dynamics it is necessary to decompose a flow variable ϕ of interest into its mean and fluctuating components as outlined in Eq. (2) where the over bar represents the mean component and the prime represents the fluctuating component.

$$\phi(x, t) = \bar{\phi}(x) + \phi'(x, t) \quad (2)$$

The time average or mean is defined by Eq. (3) and represents the sum of the variable for each time step over a maximum integration time Δt .

$$\bar{\phi}(x) = \frac{1}{\Delta t} \int_0^{\Delta t} \phi(x, t) dt \quad (3)$$

The spread of the fluctuating part $\phi'(x, t)$ around the mean $\bar{\phi}(x)$ can be described by the variance and root-mean-square (RMS) value which are defined in Eqs. (4) and (5) respectively in which $\phi(x, t)$ is the instantaneous value of the flow variable.

$$\overline{\phi'(x, t)^2} = \frac{1}{\Delta t} \int_0^{\Delta t} (\phi(x, t) - \bar{\phi}(x))^2 dt \quad (4)$$

$$\phi_{RMS} = \sqrt{\overline{\phi'(x, t)^2}} = \sqrt{\frac{1}{\Delta t} \int_0^{\Delta t} (\phi(x, t) - \bar{\phi}(x))^2 dt} \quad (5)$$

For a pulsatile flow conditions the mean or time average component of the decomposition outlined Eq. (2) is replaced with the phase average $\langle \phi \rangle(x, t)$ which is defined in Eq. (6).

$$\langle \phi \rangle(x, t) = \frac{1}{N} \sum_{n=0}^{N-1} \phi(x, t + nT) \quad (6)$$

It represents the mean value of ϕ over the number of cardiac cycles for each time point during the cycle, where N is the number of cardiac cycles and T is the period of the cardiac cycle. The updated decomposition for pulsatile flow is outlined in Eq. (7).

$$\phi(x, t) = \langle \phi \rangle(x, t) + \phi'(x, t) \quad (7)$$

The decomposition of flow variables allows for a quantitative description of the flow regime and overall behaviour. In addition to variance and RMS, the

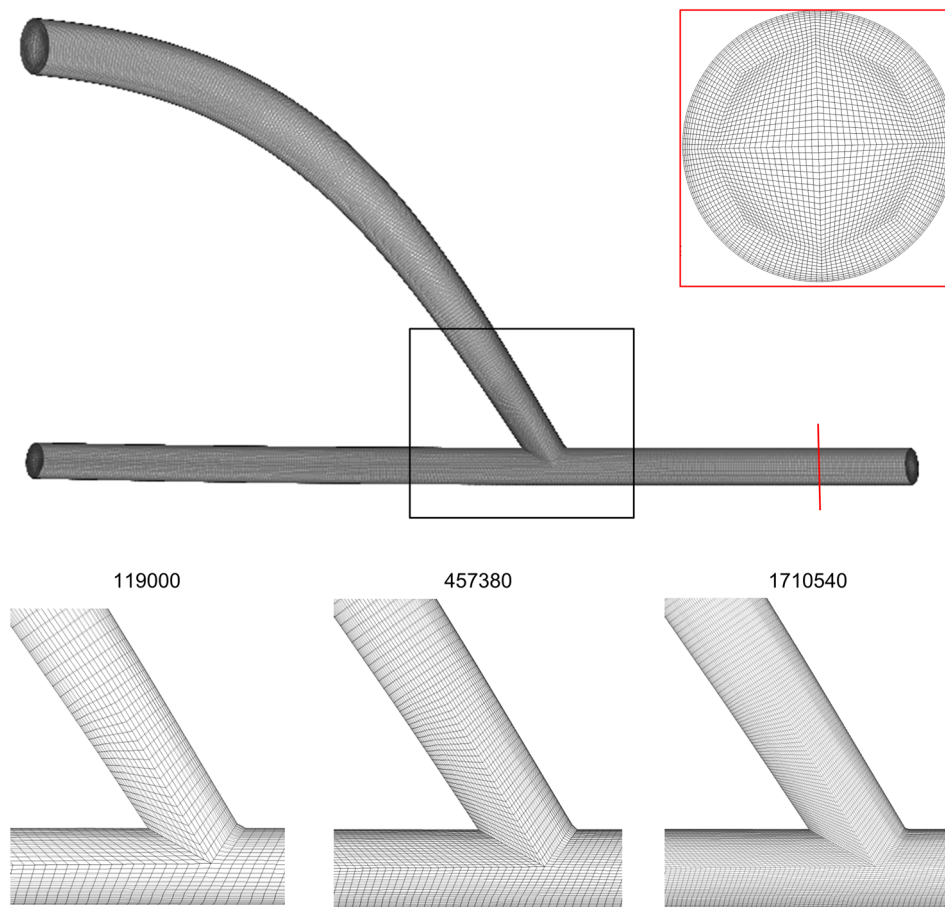


FIGURE 2. Structured hexahedral meshes of the experimental model. The highest resolution mesh utilised in this analysis is shown in plane and a cross sectional slice is shown to illustrate its radial resolution. The anastomosis areas of the three successive meshes used for grid sensitivity analysis are also shown.

skewness of velocity is also determined for this study. Skewness is a measure of the asymmetry of a variable about its mean and is defined in Eq. (8). The skewness of the velocity field was determined at a number of points along the vessels centrelines in attempt to quantify the region of flow transition.

$$Sk = \frac{1}{N} \sum_{i=1}^N \frac{V'(x, t)^3}{(V'^2)^{\frac{3}{2}}} \quad (8)$$

Both pressure and velocity fields were averaged over all time steps; the first second of data was removed to eliminate transients from solution start up and each simulation reached a physical time of 3 s. In addition to these metrics the helicity of the flow was also determined. The metric localised normalised helicity (LNH) as outlined in Eq. (9) was calculated to characterise the helical content of the bulk flow within an arteriovenous fistula. Where $v(x, t)$ and $\omega(x, t)$ are the velocity and the Vorticity vector respectively.

$$LNH = \frac{V(s, t) \cdot \omega(s, t)}{|V(s, t)| |\omega(s, t)|} \quad (9)$$

RESULTS

Numerical Results

As flow travels toward the anastomosis from the proximal artery a helical motion is created as shown. Figures 3c and 3f flow entering the anastomosis from the proximal artery undertakes a significant change in direction; it separates at the heel where a vortex with anticlockwise rotation can be seen, the flow impinges onto the opposite wall of the anastomosis creating a stagnation point which also generates a region of flow recirculation. The flow within the vein near anastomosis is disturbed and disorganised due to the sudden change in direction of the bulk flow. As flow rate

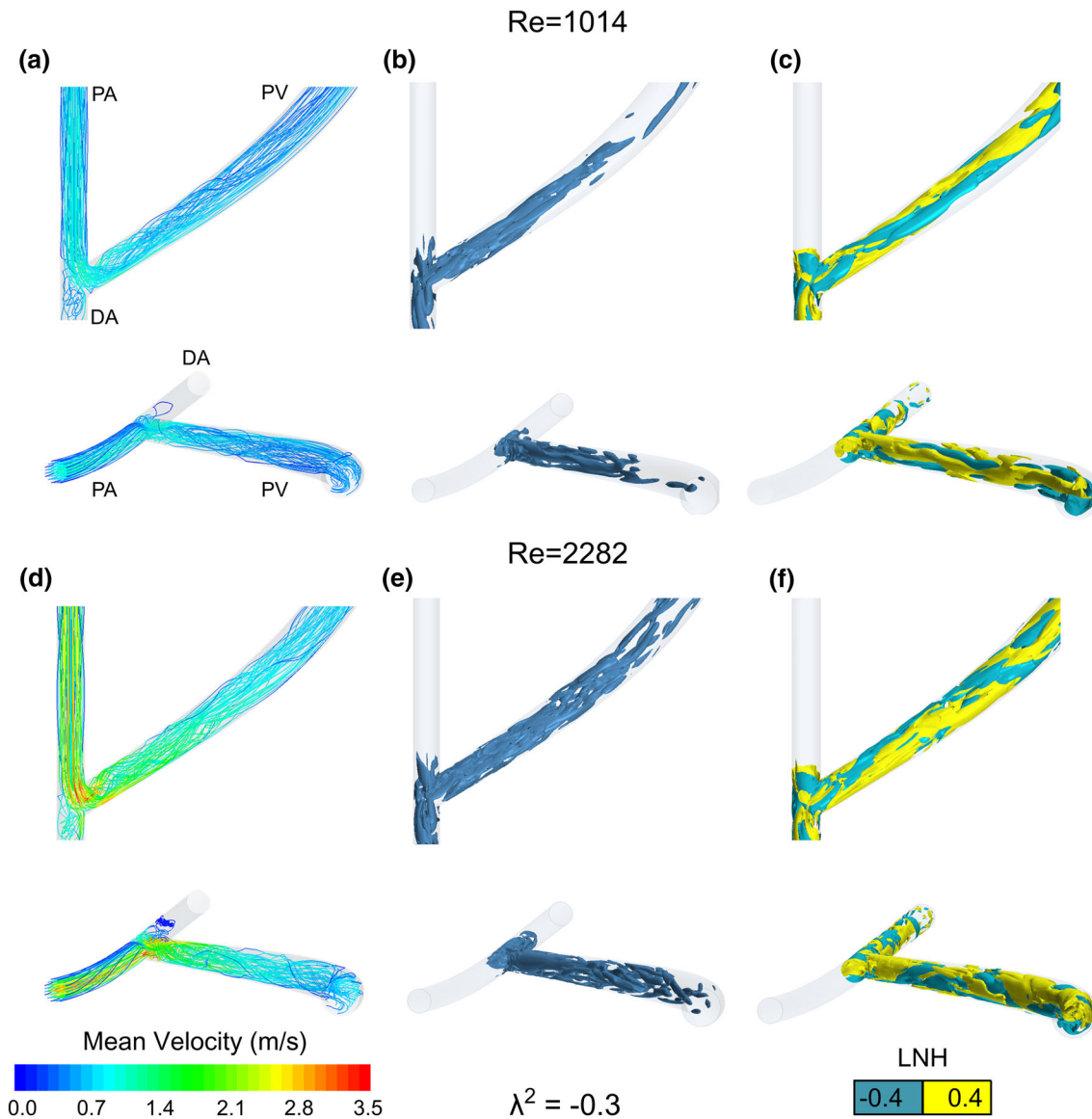


FIGURE 3. Velocity streamlines for the time averaged velocity for Reynolds numbers 1014 and 2283 corresponding to flow rates of 800 and 1800 ml/min respectively (a, d). Note the helical motion of the fluid as it moves toward the anastomosis. Visualisation of transitional flow vortices using the λ^2 criterion are shown in (b, e) and depict the extent of the instabilities which arise in the models. The value of the λ^2 -criterion is -0.3 when normalised by the mean velocity and radius of the proximal artery inlet. Isosurfaces of localised normalised helicity highlighting counter rotating fluid structures within the bulk flow are shown in (c, f) with right-handed and left handed helical structures indicated by the yellow colour (0.4) and green colour (-0.4) respectively. This figure shows that the complexity of the flow field within the anastomosis and vein increases with Reynolds number.

increases, the bulk flow in the anastomosis progressively adheres to the outer wall of the vein due to the elevated levels of vortex recirculation. A second vortex also forms in the distal artery. This is made more evident by analysing the variance of the velocity field of Figs. 4a–4d the level of the fluctuating component of velocity and the intensity of vortex recirculation increases progressively with flow, these recirculation vortices induce a restriction in the flow field and cause substantial mixing along the centreline of the vein,

these vortices cause shedding of the bulk flow and generate flow instabilities.

The plot of skewness as a function of the curvilinear abscissa in Fig. 4f depicts a spike between $s = -0.5$ and $s = 0.4$, this region between minimal and maximal values of skewness is indicative of a region of transitional behaviour or the presence of strong vortical structures. This spike coincides with an area of increased vortex shedding with enhanced mixing. Therefore, this analysis identifies that instabilities

TABLE 3. Discretisation error of the TAWSS over the vascular surface and the pressure drop across the fistula.

	Structured hexahedral		Unstructured hybrid tetrahedral	
	$\Phi = \text{TAWSS}$	$\Phi = \text{Pressure drop}$	$\Phi = \text{TAWSS}$	$\Phi = \text{Pressure drop}$
N_1	1,710,540	1,710,540	2,041,977	2,041,977
N_2	457,380	457,380	583,079	583,079
N_3	119,000	119,000	173,373	173,373
r_{21}	1.55	1.55	1.519	1.519
r_{32}	1.57	1.57	1.498	1.498
Φ_1	12.6271	22.04	11.220	18.290
Φ_2	12.1803	21.99	11.047	19.016
Φ_3	12.1715	22.27	10.888	19.594
P	8.73	3.82	0.28	0.63
ϕ_{ext}^{21}	12.6370	22.051	12.611	21.511
θ_1^{21}	3.54%	0.23%	1.54%	2.95%
e_{ext}^{21}	0.08%	0.05%	11.03%	8.91%
GCI_{fine}^{21}	0.10%	0.06%	15.5%	12.23%

originate within the anastomosis prior to advecting into the venous outflow. The intensity or level of the fluctuations reduces further away from the anastomosis and the flow will return to a stable state. However, this position or point is dependent on the Reynolds number of the flow as shown in Figs. 3b, 3e and 4a–4d and is not indicated by the measure of skewness.

Grid Convergence Results

Simulations using steady inflow boundary conditions were conducted for a flow rate of 1800 ml/min corresponding to values near systolic peak for the pulsatile analysis. The structured hexahedral mesh described previously was compared against an unstructured hybrid mesh consisting of prismatic boundary elements near walls and tetrahedral elements elsewhere. Quantitative grid convergence was assessed based on a grid convergence index (GCI), which accounts for the degree of grid refinement.⁶ Further details are provided in Supplementary Material. Successive meshes with a refinement factor greater than 1.5 were used; these meshes consisted of 0.119×10^6 , 0.457×10^6 and 1.710×10^6 hexahedral elements compared to 0.173×10^6 , 0.583×10^6 and 2.041×10^6 hybrid elements. Wall shear stress is a critical quantity with respect to grid convergence.¹⁴ Therefore, the WSS magnitude was chosen as term of comparison of the grids, it was analysed by using the surface averaged value over an integration time of 2 s. The numerical uncertainty in the fine grid solution for the time averaged wall shear stress (TAWSS) on the lumen surface is reported as 0.10 and 15.5% for the hexahedral and hybrid tetrahedral meshes respectively. Table 3 quantifies the relative error and GCI for each consecutive refinement. The numerical uncertainty in the fine grid solution for pressure drop is reported as 0.06% for the hexahedral mesh compared to 12.23%

for the hybrid mesh. To assess temporal sensitivity the CGI analysis was repeated for solutions with time steps of 1, 0.5, and 0.25 ms. The numerical uncertainty in the fine grid solution for TAWSS was 2.0, 0.10 and 0.68% for the 1, 0.5, and 0.25 ms solutions respectively. The 0.5 ms was chosen as GCI was below 1% and required less computational time compared to the 0.25 ms solution. Full details of these results are provided in Supplementary Material 1.

Experimental vs. Numerical Pressure Drop

Steady Boundary Conditions

At higher Reynolds numbers the flow becomes more unstable with enhanced vortex shedding which is evidenced by the larger levels of fluctuations within the anastomosis and outflow vein. It is interesting to note the influence of these instabilities on the pressure drop as shown in Fig. 5a in which there is substantial variation about the mean. The fluctuating component of the pressure drop signal was autocorrelated for mean flow rates 1100, 1400 and 1800 ml/min and were found to be random and non-periodic, more detail is provided in supplementary material 1. Pressure drop vs. flow rate is presented in Fig. 5b. The plot demonstrates that there is a quadratic relationship between pressure drop and flow rate across the anastomosis. The majority of experimental values lie within the standard deviation range of the numerical pressure drops even for the coarser mesh and overall there is good agreement between numerical and experimental measures for the steady boundary condition. From the grid convergence analysis it is apparent that the coarsest solution provides an accurate estimate of the mean pressure drop (Table 3). However, at higher Reynolds numbers high resolutions are recommended in the presence of secondary vortices and will provide a more accurate measurement of the mean

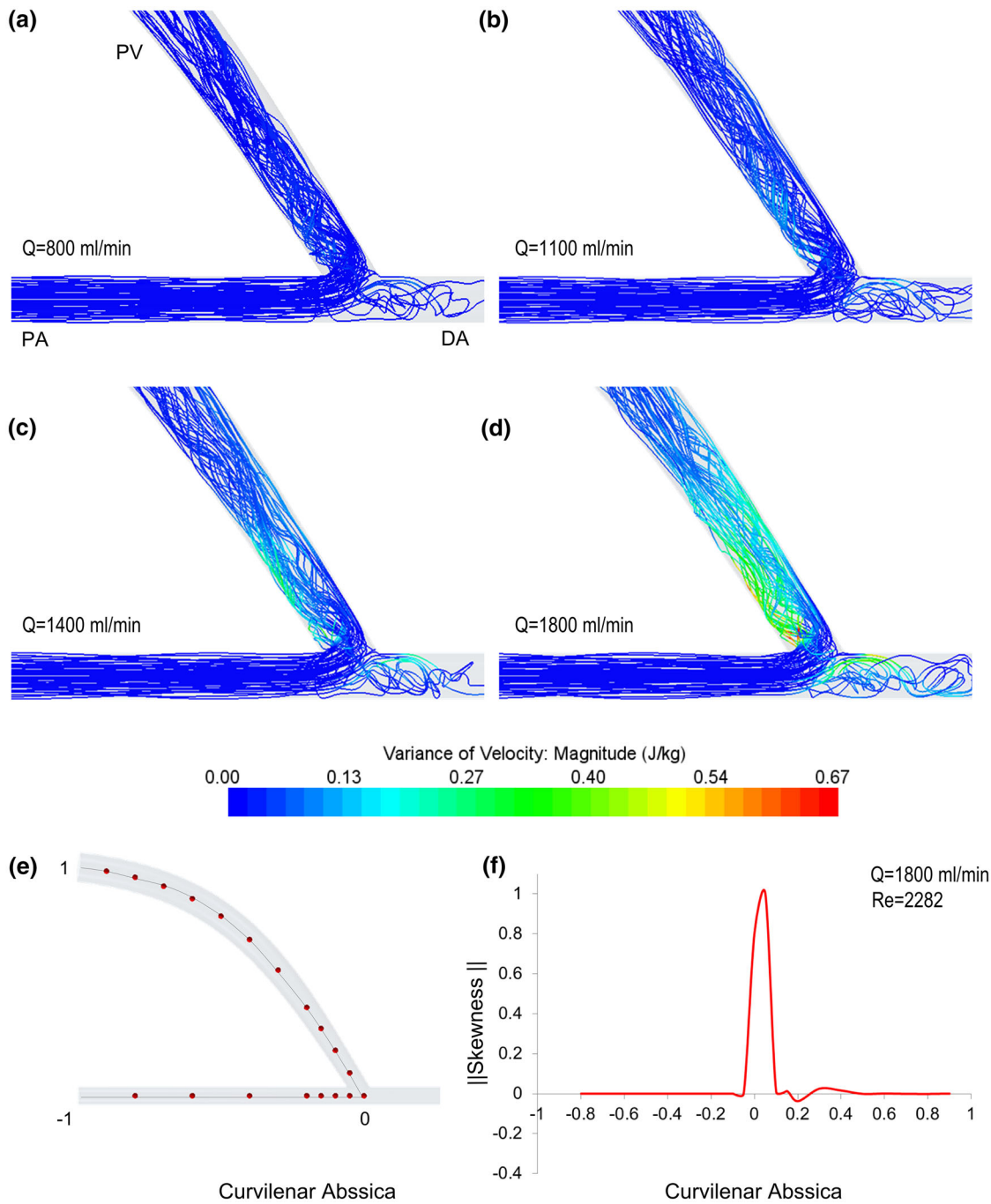


FIGURE 4. Streamlines of the variance of the velocity solutions are presented in (a–d) for flow rates 800, 1100, 1400, and 1800 ml/min respectively. Note that the flow in the proximal artery is stable even at the largest flow rate. The level or intensity of the velocity fluctuations increases progressively with flow rate. The probe locations of the velocity field are shown in (e) and the skewness of the velocity field for $Re = 2282$ is shown in (f). The measure was normalised by the maximum value within the range.

flow. The uncertainty analysis of wall shear stress highlights the influence of mesh resolution more clearly as this dynamic parameter is a function of the velocity gradient.

Pulsatile Boundary Conditions

To compare the steady state solutions against pulsatile results the cycle averaged values for velocity and pressure drop over the anastomosis were determined.

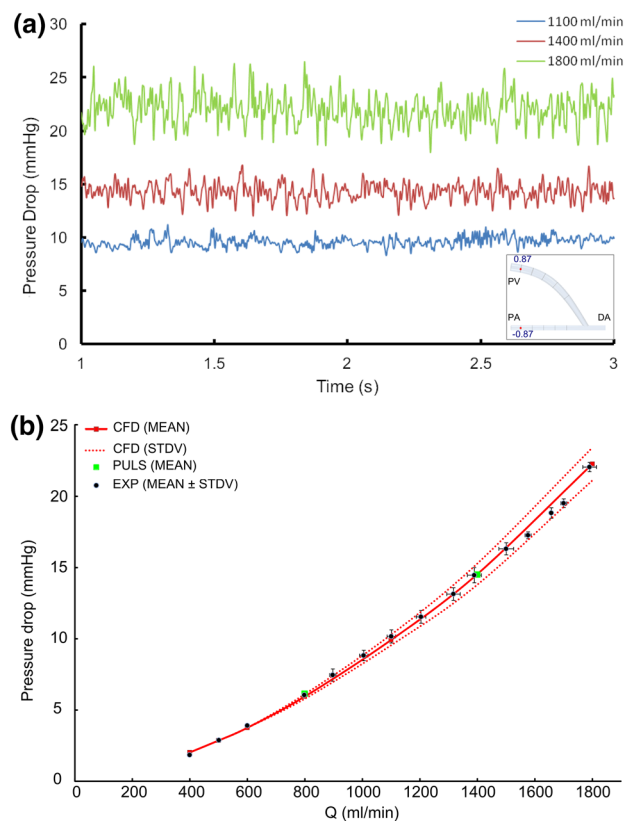


FIGURE 5. (a) Numerical pressure drop vs. time for steady boundary conditions corresponding to flow rates of 1100, 1400 and 1800 ml/min respectively between -0.87 and 0.87 of the curvilinear abscissa. Note that high frequency oscillations dominate the signals. Simulations were run for 18–30 flow through times. Pressure drop across the anastomosis vs. flow rate for the coarsest mesh of 120 k cells is presented in (b). The cycle averaged pressure drop for mean flow rates of 800 and 1400 ml/min are shown to compare the steady state results against the pulsatile boundary conditions.

The first cycle was removed from the analysis to eliminate transients from solution start-up. 2000 time steps per cycle are performed for a mean flow rate of 800 and 1400 ml/min respectively and solutions are obtained on the finest 1700 k element mesh. Figure 5 highlights that the pressure drop determined with steady boundary conditions are comparable to the cycle averaged pressure drop for the same mean flow rate which infers that the pressure drop across an anastomosis can be determined with steady inflow conditions. The influence of pulsatility on the velocity field is examined in Fig. 6. The figure depicts the variation in the velocity signal along the length of the arterial and venous centrelines for a mean flow rate of 1400 ml/min. There is a significant increase in the level of fluctuations as flow approaches the anastomosis and within the outflow vein, the intensity of these fluctuations and the pulsatility of the flow reduce further away from the anastomosis within the vein. It is evident that instabilities persist throughout the cardiac cycle

within the anastomosis and swing segment of the vein due to the aperiodic nature of the velocity signal in these areas. Analysing the root mean square and power spectrum of these signals can reveal substantial information about the nature and character of the flow. Figure 7 illustrates this analysis for a point directly positioned in the anastomosis. The velocity signals are computed over the two cardiac cycles. The spectral energy at frequencies <16 Hz are associated with the cardiac cycle frequencies which clearly dominate the signal as shown in Fig. 7a. The significant energy beyond this range is associated with the instabilities within the anastomosis as indicated in Fig. 7b. The deviations from the phase-averaged velocity are shown in Fig. 7d. The root mean square of the velocity signal is 0.12 m/s corresponding to a fluctuation of 9.3% of the mean velocity at this location. The power spectrum of the velocity signal displays a broad bandwidth with significant energy between 100 and 300 Hz; the high frequency content of the velocity field at this point indicates the presence of instabilities and the power spectrum displays an energy cascade at these high frequencies as illustrated in Fig. 7b which is suggestive of unstable flow and irregular behaviour. It is interesting to note that flow instabilities are most prominent during peak systole but also persist through much of or even all of diastolic phase of the cycle which is clearly indicated in Fig. 7d in which the phase average velocity is removed. Likewise for the pressure signal as shown in Fig. 8, the pressure fluctuations during the diastolic phase are similar to those achieved with steady inflow conditions. This may be attributed to the longer time that instabilities have to develop during the diastolic phase of the cycle. Intuitively this field of thought would explain the relative smoothness of the pressure signal and absence of such oscillations during the acceleration phase of systole.

DISCUSSION

The verification study was performed on a representative model of an arteriovenous fistula for a range of flow rates which are seen *in vivo* after fistula formation. This study demonstrates that the solution strategy adopted to solve the unsteady incompressible Navier–Stokes equations is capable of capturing the main flow features within an arteriovenous fistula and is able to reproduce the pressure drop across it even on the coarsest mesh. This non-linear pressure drop is related to the inflow Reynolds number and the cross sectional area of the anastomosis junction which in turn is determined by the angle and diameter ratio of the vessels. The influence of these geometrical parameters on the velocity field will dictate the pressure drop.¹⁸

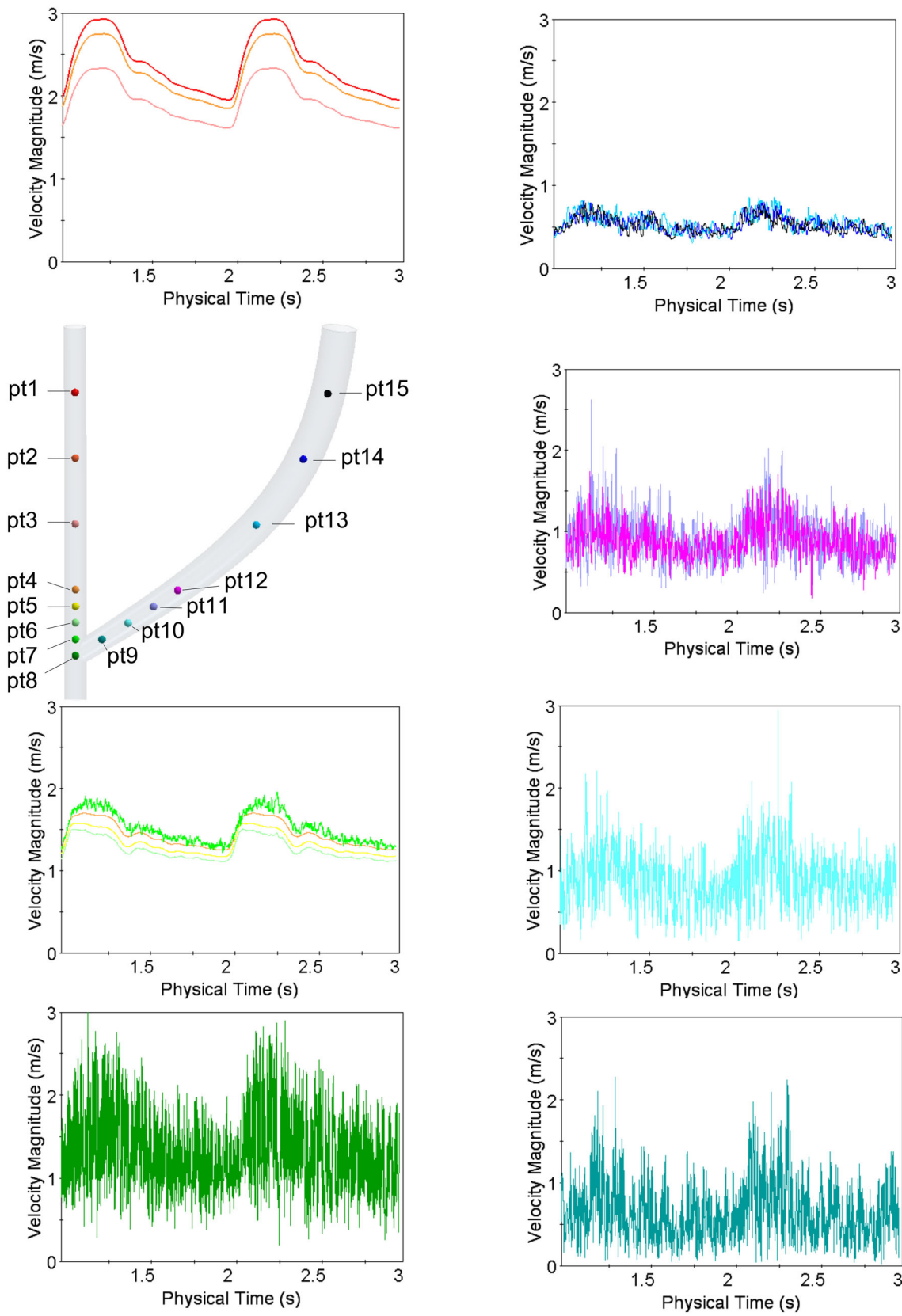


FIGURE 6. Velocity–time trace histories along centreline points (pt1–pt15) within the fistula model for a pulsatile flow solution with a mean flow rate of 1400 ml/min over the finest 1700 k element mesh with a time step of 5×10^{-4} s.

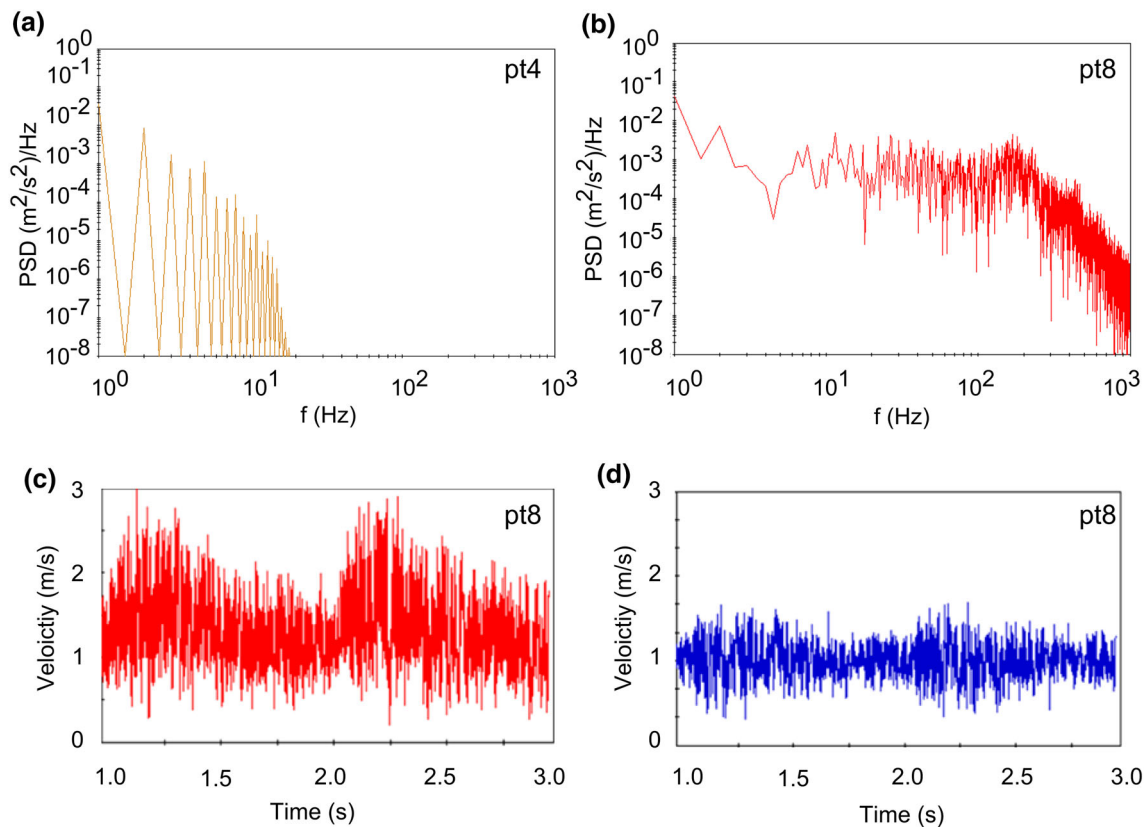


FIGURE 7. The stream-wise velocity power spectrum vs. frequency is presented for points 4 and points 8 as illustrated in (a) and (b) respectively. The Velocity magnitude for two cardiac cycles for point 8 which is within the anastomosis is shown in (c). Note the aperiodic nature of the velocity signal. This time signal with the phase average velocity removed is shown in (d).

Instabilities are found to develop within the anastomosis junction prior to advecting into the outflow vein under both steady and pulsatile flow conditions. The sudden change in the flow direction at the anastomosis induces instabilities which produce high frequency fluctuations in the pressure drop signal. The intensity of fluctuations is greatest in the anastomosis junction and becomes reduced further away from the junction. The flow field becomes highly disturbed with multiple vortices of various sizes passing through the outflow vein. This analysis is similar to that of Sivanesan *et al.*, who observed high levels of turbulent intensity near the anastomosis and a reduction in the level along the length of the venous section¹⁷ The assumption that the flow regime is laminar based on the Reynolds number range for a straight pipe is not applicable to a fistula. Laminar flow is well ordered, with particles travelling in parallel non mixing layers similar to the flow pattern in the proximal artery. However, as flow moves toward and across the anastomosis it becomes disorganised and there is significant mixing between fluid layers which is indicative of unstable flow. The measure of skewness provided a quantifiable method to locate the point or onset of flow instabilities within the fistula and provides

a means to isolate some of the mechanisms involved in the breakdown process of the flow field. Consequently, it is not a direct indication of transitional to turbulent flow. Instead, analysing the power spectrum density of the velocity and pressure signals confirmed whether the signal is unstable. The frequency spectrum often includes three distinct ranges. The first range contains energy of the driving flow and spatially corresponds to large scale eddies, the second part is referred to as the inertial subrange where energy cascades from the large scales toward small scales, the spectrum slope is characterised by a constant value of $-5/3$ following the well known Kolmogorov law. The third part is the viscous dissipation subrange corresponding to high-frequency turbulent motions and the transfer or dissipation of energy at the smallest spatial and temporal scales. Higher Reynolds number and turbulent flows are often identified as the inertial subrange would occupy or encompass a large range of frequencies. Increased spectral energy in the range of 100–500 Hz has been found to indicate transitional and turbulent flow *in vivo*.¹³ The presence of significant energy associated with high frequency content of the signal (100–300 Hz) indicated unstable flow in this analysis. It is important

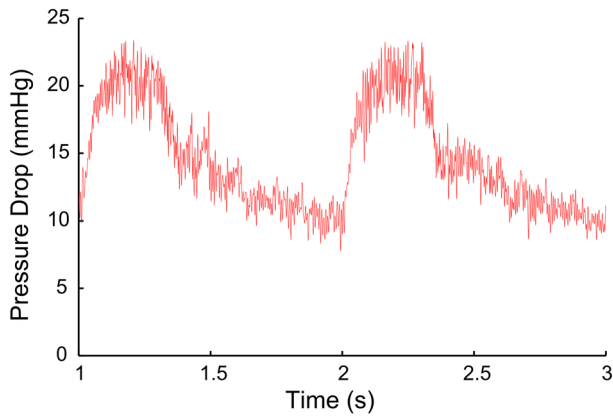


FIGURE 8. Pressure drop vs. time for a mean flow rate of 1400 ml/min over two cardiac cycles obtained on the finest 1700 k element mesh with a time step of 5×10^{-4} s.

to note that in this study, a fine spatial and temporal resolution CFD simulation was employed. However, this model did not attempt or intend to fully resolve the smallest temporal or spatial scales of turbulent motion, but rather the scales with the most energy. Analysing the effects of pulsatile flow it is clear that it doesn't significantly alter the relationship between pressure drop and flow rate. These findings are in agreement with those of Botti *et al.*,³ The pressure drop signal comprises of high frequency oscillations which are in phase with the low forcing frequencies of the cardiac cycle. The flow instabilities are most pronounced during peak systole but persist through much of or even all of diastole. The significant drop in potential energy across the anastomosis must be transferred or converted to maintain the principle of energy conservation. In this analysis the drop coincided with the onset of unstable flow. For Reynolds numbers within the normal *in vivo* range, instabilities in the flow field caused high frequency oscillations in the pressure drop across the anastomosis. These rapid temporal variations in pressure could give rise to a palpable thrill that is felt across the anastomosis. Previous studies have reported significant *in-vivo* measurements of vein wall motion in the range of 100–200 Hz for an arteriovenous graft in porcine and canine subjects.^{10,12} It is also interesting to note the presence of fluctuations greater than 100 Hz for both velocity and pressure within the anastomosis of this analysis. These frequencies are in a similar bandwidth to bruits and thrills and although no direct correlation can be made in this analysis, for a functioning fistula, bruits and thrills are known to persist at systole and throughout diastole similar to the fluctuations of velocity and pressure under pulsatile conditions.¹ Variations in the intensity and duration of the bruit or thrill are often utilised to assess for vascular lesions. This aspect of the analysis is interesting on many fronts as it

could be suggestive that these rapid fluctuations in the velocity and pressure field could lead to dilation of the outflow vein similar to the proposed theory of post-stenotic dilation.¹³ Therefore, the combination of high shear stress and pressure fluctuations could instigate outward remodelling of the vein. Equally though, the synergistic effects of these instabilities with areas of recirculation could cause inward remodelling of the vein. Hence, there is a need to assess and capture these dynamics of the flow field. As a result larger spatial and temporal resolutions are needed. Monitoring changes in the intensity of these fluctuations could also be used to assess for the presence or onset of vascular lesions within the outflow vein.

Limitations

It is important to note that the max integration time and number of cycles used in this preliminary study of flow instabilities are substantially small therefore, statistical reliability cannot be assured. Hence, this numerical model only offers an estimate of the statistically relevant flow behaviour, yet it appears to be able to replicate mean flow features with relative accuracy. Despite this, these averaging methods only allow for an estimate of the intensity of the fluctuations and overall flow behaviour. The influence of pressure and velocity fluctuations on wall motion or stretch could not be assessed due to the assumption of a rigid wall in the analysis. Therefore, no direct correlation to thrills or bruits could be undertaken. In addition, AVF creation is known to alter cardiac function *in vivo*, whether instabilities are sustained as consistently as *in vitro* and *in silico* models is unclear. Although, the representative model employed in this analysis is derived from patient specific characteristics we acknowledge that the representative model is unable to replicate the exact shape and profile of the anastomosis area or capture the tortuosity of the venous segment or the heterogeneous variation in the diameter that can occur. Further geometric characterisation of fistula morphology is needed, a robust characterisation may lead to an independent measure of risk of non-maturation as surgical configuration may limit IH prone regions.² We acknowledge the use of one case as a limitation of this study, the acquisition of patient specific flow rates and geometries of AVFs within the same sampling window are needed to observe trends and traits amongst the population of patients with fistulae.

CONCLUSION

Unstable flow in an arteriovenous fistula has been documented *in vitro* and clinically detected *in vivo*. This study highlights that adequately resolved CFD can be

used to replicate these instabilities *in silico*. This study also verified that the pressure drop across an anastomosis *in vitro* could be replicated by computational models. The pressure drop across the anastomosis exhibits a quadratic relationship for both steady and pulsatile inflow boundary conditions. The resistance of the anastomosis is dictated by its geometrical configuration and its flow rate. Instabilities arise within the anastomosis and are present throughout the outflow vein resulting in distorted and unstable flow behaviour. Although the representative geometry of an AVF employed in this study allowed for an analysis of flow features, the consequences of these dynamics remain to be identified. Therefore, the application of adequately resolved solutions such as those employed in this study to image based longitudinal studies allows for important features to be characterised and their implications on pathological remodelling to be assessed non-invasively. This will help towards increasing our understanding of the mechanisms which elicit positive and negative remodelling within fistulae. Identifying metrics associated with risk of non-maturation have a significant interest in the clinical realm in terms of early intervention and improving fistula outcomes.

ELECTRONIC SUPPLEMENTARY MATERIAL

The online version of this article (doi: [10.1007/s13239-015-0246-6](https://doi.org/10.1007/s13239-015-0246-6)) contains supplementary material, which is available to authorized users.

CONFLICT OF INTEREST

All authors declare that they have no conflict of interest.

STATEMENT ON HUMAN AND ANIMAL STUDIES

No human studies were carried out by the authors for this article. No animal studies were carried out by the authors for this article.

REFERENCES

- ¹Asif, A., P. Roy-Chaudhury, and G. A. Beathard. Early arteriovenous fistula failure: a logical proposal for when and how to intervene. *Clin. J. Am. Soc. Nephrol.* 1:332–339, 2006.
- ²Bharat, A., M. Jaenicke, and S. Shenoy. A novel technique of vascular anastomosis to prevent juxta-anastomotic stenosis following arteriovenous fistula creation. *J. Vasc. Surg.* 55:274–280, 2012.
- ³Botti, L., K. Canneyt, R. Kaminsky, T. Claessens, R. N. Planken, P. Verdonck, A. Remuzzi, and L. Antiga. Numerical evaluation and experimental validation of pressure drops across a patient-specific model of vascular access for hemodialysis. *Cardiovasc. Eng. Technol.* 4:485–499, 2013.
- ⁴Browne, L. D., P. Griffin, K. Bashar, S. R. Walsh, E. G. Kavanagh, and M. T. Walsh. In vivo validation of the *in silico* predicted pressure drop across an arteriovenous fistula. *Ann. Biomed. Eng.* 43:1275–1286, 2015.
- ⁵Carroll, G. T., T. M. McGloughlin, P. E. Burke, M. Egan, F. Wallis, and M. T. Walsh. Wall shear stresses remain elevated in mature arteriovenous fistulas: a case study. *J. Biomech. Eng.* 133:021003, 2011.
- ⁶Celik, I. B., U. Ghia, P. J. Roache, and C. J. Freitas. Procedure for estimation and reporting of uncertainty due to discretization in CFD applications. *J. Fluids* 130(7) 2008.
- ⁷Cheng, N. S. Formula for the viscosity of a glycerol-water mixture. *Ind. Eng. Chem. Res.* 47:3285–3288, 2008. doi: [10.1021/ie071349z](https://doi.org/10.1021/ie071349z).
- ⁸Ene-Iordache, B., and A. Remuzzi. Disturbed flow in radial-cephalic arteriovenous fistulae for haemodialysis: low and oscillating shear stress locates the sites of stenosis. *Nephrol. Dial. Transplant.* 27:358–368, 2012.
- ⁹Fillinger, M. F., E. R. Reinitz, R. A. Schwartz, D. E. Resetarits, A. M. Paskanik, D. Bruch, and C. E. Bredenberg. Graft geometry and venous intimal-medial hyperplasia in arteriovenous loop grafts. *J. Vasc. Surg.* 11:556–566, 1990.
- ¹⁰Lee, S., P. Fischer, F. Loth, T. Royston, J. Grogan, and H. Bassiouny. Flow-induced vein-wall vibration in an arteriovenous graft. *J. Fluids Struct.* 20:837–852, 2005.
- ¹¹Lee, S.-W., D. S. Smith, F. Loth, P. F. Fischer, and H. S. Bassiouny. Importance of flow division on transition to turbulence within an arteriovenous graft. *J. Biomech.* 40:981–992, 2007.
- ¹²Loth, F., P. F. Fischer, N. Arslan, C. D. Bertram, S. E. Lee, T. J. Royston, W. E. Shaalan, and H. S. Bassiouny. Transitional flow at the venous anastomosis of an arteriovenous graft: potential activation of the ERK1/2 mechanotransduction pathway. *J. Biomech. Eng.* 125:49–61, 2003.
- ¹³McGah, P. M., D. F. Leotta, K. W. Beach, J. J. Riley, and A. Aliseda. A longitudinal study of remodeling in a revised peripheral artery bypass graft using 3D ultrasound imaging and computational hemodynamics. *J. Biomech. Eng.* 133:041008, 2011.
- ¹⁴Pustjens, L. W. J. Three-dimensional modeling to derive the pressure drop-flow relation at an AertioVenous Fistula. M.S. Thesis, Eindhoven University of Technology, 2013.
- ¹⁵Rajabi-Jagahrgh, E., M. K. Krishnamoorthy, Y. Wang, A. Choe, P. Roy-Chaudhury, and R. K. Banerjee. Influence of temporal variation in wall shear stress on intima-media thickening in arteriovenous fistulae. *Semin. Dial.* 26:511–519, 2013.
- ¹⁶Sigovan, M., V. Rayz, W. Gasper, H. F. Alley, C. D. Owens, and D. Saloner. Vascular remodeling in autogenous arterio-venous fistulas by MRI and CFD. *Ann. Biomed. Eng.* 41:657–668, 2013.
- ¹⁷Sivanesan, S. Flow patterns in the radiocephalic arteriovenous fistula: an *in vitro* study. *J. Biomech.* 32:915–925, 1999.
- ¹⁸Van Canneyt, K., T. Pourchez, S. Eloit, C. Guillaume, A. Bonnet, P. Segers, and P. Verdonck. Hemodynamic impact of anastomosis size and angle in side-to-end arteriovenous fistulae: a computer analysis. *J. Vasc. Access* 11:52–58, 2010.